*Progress In Electromagnetics Research C, Vol. 17, 79–94, 2010*

# SPIKING NEURAL NETWORKS FOR BREAST CANCER CLASSIFICATION USING RADAR TARGET SIGNATURES

**B. McGinley, M. O'Halloran, R. C. Conceição, F. Morgan M. Glavin and E. Jones** †

College of Engineering and Informatics
National University of Ireland Galway
University Road, Galway, Ireland

**Abstract**—Recent studies have shown that the dielectric properties of normal breast tissue vary considerably. This dielectric heterogeneity may mean that the identification of tumours using Ultra Wideband Radar imaging alone may be quite difficult. Significantly, since the dielectric properties of benign tissue were shown to overlap with those of malignant, breast tumour classification using traditional UWB Radar imaging algorithms could be very problematic. Rather than simply examining the dielectric properties of scatterers within the breast, other features of scatterers must be used for classification. Radar Target Signatures have been previously used to classify tumours due to the significant difference in size, shape and surface texture between benign and malignant tumours. This paper investigates Spiking Neural Networks (SNNs) applied as a novel tumour classification method. This paper will describe the creation of 3D tumour models, the generation of representative backscatter, the application of a feature extraction method and the use of SNNs to classify tumours as either benign or malignant. The performance of the SNN classifier is shown to outperform existing UWB Radar classification algorithms.

*Received 2 October 2010, Accepted 20 October 2010, Scheduled 4 November 2010*
Corresponding author: Martin O'Halloran (martin.ohalloran@gmail.com).
† All the authors are also with Bioelectronics Research Cluster, National Centre for Biomedical Engineering Science (NCBES), National University of Ireland Galway, University Road, Galway, Ireland.

## 1. INTRODUCTION

Breast cancer is one of the most common cancers to affect women. In the United States alone, it accounts for 31% of new cancer cases, and is second only to lung cancer as the leading cause of deaths in American women [1]. More than 184.000 new cases of breast cancer are diagnosed each year resulting in approximately 41.000 deaths. Early detection and intervention is one of the most significant factors in improving the survival rates and quality of life experienced by breast cancer sufferers [2], since this is the time when treatment is most effective.

The current standard screening method for detecting non-palpable early stage breast cancer is X-ray mammography. Despite the fact that X-ray mammography provides high resolution images using relatively low radiation doses, its limitations are well documented [2]. The search for new imaging techniques is motivated by the need for increased specificity and sensitivity, especially in the case of radiographically dense tissue. In younger women in particular, breast tissue typically presents a higher dense-to-fatty tissue ratio and malignancies occurring in dense-tissue breasts are statistically more likely to be missed by X-ray mammography [3]. In the US, between 4%–34% of all breast cancers are missed by conventional mammography [4], while 70% of all malignancies identified are found to be benign after biopsy [5]. These false positive conclusions result in unnecessary biopsies, causing considerable distress to the patient and an unnecessary financial burden on the health service [5, 6].

Three alternative active microwave imaging techniques are under development, Hybrid Microwave-Induced Acoustic imaging, Microwave Tomography and Ultra-Wideband (UWB) Radar imaging. The hybrid imaging method involves heating any tumours present in the breast using microwave signals, and using ultrasound transducers to record the resultant pressure waves due to the heat-induced expansion of the tumour tissue. Based on these recorded waves, the presence and location of the tumours can be identified [7–9]. Microwave Tomography involves reconstructing the complete dielectric profile of the breast using a forward and inverse scattering model [10–13]. Finally, Ultra-Wideband (UWB) Radar imaging, as proposed by Hagness et al. [14], uses reflected UWB signals to determine the location of microwave scatterers within the breast. This is a similar imaging procedure to that used in surface-penetrating radar [15]. Rather than using the tomographic approach of reconstructing the entire dielectric profile of the breast, UWB radar imaging uses the Confocal Microwave Imaging (CMI) approach [14] to identify and locate regions of scatterings within the breast [16–24].

However, a recent study of the dielectric properties of adipose, fibroglandular and cancerous breast tissue has highlighted the dielectric heterogeneity of normal breast tissue [25, 26]. Significantly, rather than the dielectric properties of normal breast tissue being primarily homogeneous, Lazebnik et al. found a very significant dielectric contrast between adipose and fibroglandular tissue within the breast. The dielectric properties of adipose tissue was found to be lower than any previously published data for normal tissue. Conversely, the dielectric properties of fibroglandular tissue was found to be significantly higher than any previously published data for normal breast tissue. This heterogeneity of normal breast tissue had been considerably underestimated in more historical studies, and the difficultly this presents to existing data-independent beamformers has been examined by the authors previously [27].

In order to improve sensitivity and specificity in the dielectrically heterogeneous breast, more robust methods need to be developed to classify tumours as either benign or malignant. Several studies have examined the use of Radar Target Signatures (RTS) to classify scatterers within the breast [28–35]. In this paper, a novel classification method using Spiking Neural Networks (SNN) is presented. The structure of the remainder of the paper is as follows: Section 2 describes the generation of realistic tumour models and corresponding FDTD simulations; Section 3 describes the SNNs, Section 4 describes the experimental setup, while Section 5 describes the results and corresponding conclusions.

## 2. TUMOR MODELING

### 2.1. Gaussian Random Spheres

Tumours present different physical characteristics based on their nature, i.e., whether they are benign or malignant. The most relevant features from the perspective of UWB imaging are size, shape and texture of surface, as these are characteristics that most significantly influence the RTS of tumours. Benign tumours typically have smooth surfaces and have spherical, oval or at least well-circumscribed contours. Conversely, malignant tumours usually present rough and complex surfaces with spicules or microlobules, and their shapes are typically irregular, ill-defined and asymmetric [36]. In this study, the primary concern is the analysis of small tumours (up to 1 cm in radius). Shape and texture of the surface of a tumour are the two most important characteristics that will help differentiate between a benign and a malignant tumour. The tumour models are based on the Gaussian Random Spheres (GRS) method [37, 38]. GRS can

be modified mathematically to model both malignant and benign tumours by varying the mean radius $\alpha$ and the covariance function of the logarithmic radius. The shape is determined by the radius vector, $\mathbf{r} = r(\theta, \psi)$, is described in spherical coordinates $(r, \theta, \psi)$ by the spherical harmonics series for the logradius $s = s(\theta, \psi)$:

$$r(\theta, \psi) = \alpha \exp\left[s(\theta, \psi) - \frac{1}{2}\beta^2\right] \tag{1}$$

$$s(\theta, \psi) = \sum_{l=0}^{\infty} \sum_{m=-l}^{l} s_{lm} Y_{lm}(\theta, \psi) \tag{2}$$

In the equations above, $\beta$ is the standard deviation of the logradius, $s_{lm}$ are the spherical harmonics coefficients and $Y_{lm}$ are the orthonormal spherical harmonics. Three different tumour models at two different sizes are considered in this paper. Malignant tumours are represented by spiculated and microlobulated GRS, whereas benign tumours are modelled by smooth GRS. Microlobulated and smooth GRS are obtained by varying the correlation angle from low to high. Spiculated

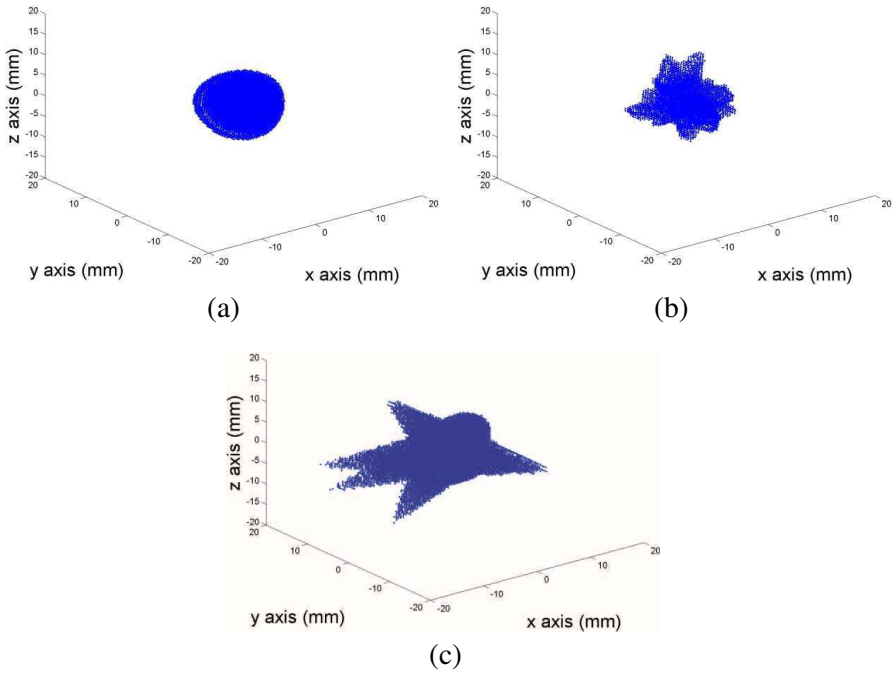


**Figure 1.** (a) Benign, (b) microlobulated, and (c) malignant tumour model.

GRS are obtained by adding 3, 5 or 10 spicules to smooth GRS. The average radius of all types of spheres are 2.5 and 7.5 mm. Between all sizes and shapes, the number of tumour models developed was 368. A sample of each of the types tumour models is shown in Figure 1.

### 2.2. FDTD Model

The tumours are placed in a 3D Finite-Difference Time-Domain (FDTD) model. The FDTD model has a 0.5 mm cubic grid resolution and the backscattered signals were generated through a Total-Field/Scattered-Field (TF/SF) structure, in which the tumours are completely embedded in the Total Field (TF) [33, 35]. The TF/SF region has the following dimensions: the Scattered Field (SF) is a square geometric prism with square bases measuring 153.5 mm on the side and the height measuring 137.5 mm. The TF is located at the centre of the SF and is represented by a 50 mm-sided cube (the origin of the SF and the TF are at the point $(0, 0, 0)$ mm). The dielectric properties of both adipose and cancerous breast tissue are incorporated using a Debye model, based on the dielectric properties established by Lazebnik et al.. The TF/SF region is terminated with a 6 mm-layer Uniaxial Perfectly Matched Layer (UPML) which suppresses any boundary reflections [39].

A pulsed plane wave is transmitted towards the target from four different equidistant angles (0, 90, 180 and 270°) and the resulting cross-polarized backscatter is recorded and analysed from four observation points located at: $(0, 0, -74)$, $(-74, 0, 0)$, $(0, 0, 74)$ and $(74, 0, 0)$ mm in $(x, y, z)$ axes. The incident pulse is a modulated Gaussian pulse with center frequency at 6 GHz where the 1/e full temporal width of the Gaussian envelop was 160 ps. For two transmitters, the pulse is linearly polarized in the $x$-$y$ plane and transmitted in the $z$ direction, and for the remaining transmitters, the pulse is polarized in the $y$-$z$ plane and transmitted in the $z$ direction. Each observation point is located in the Scattered Field at a distance of 74 mm from the center of the tumour, which is located at the centre of the Total Field. The acquired backscattered recorded signals are then downsampled from 1200 GHz to 75 GHz. Figure 2 shows a representation of the TF/SF grid, with the location of the origin of the first incident plane wave and respective observer point as well as the position of the tumour.

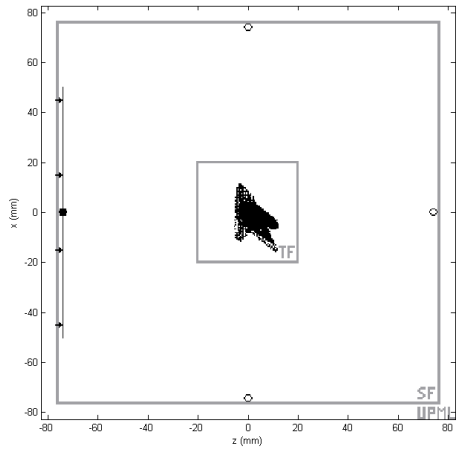


**Figure 2.** Cross-section of the 3D FDTD space lattice partitioned into Total Field (TF), Scattered Field (SF) and UPML regions, for a homogeneous breast model. The target, a spiculated tumour located at the centre of the TF in this example, is illuminated by a pulsed plane wave propagating in the $+z$ direction (represented by a dark line) and backscatter is recorded at the first observer location: $(0, 0, -74)$ mm (represented by a filled circle). All four observation points are represented by small circles in the image.

## 3. SPIKING NEURAL NETWORKS & GENETIC ALGORITHMS

### 3.1. Spiking Neural Network

The fundamental processing units in the organic central nervous system are neurons which are interconnected in a complex pattern [40]. The current understanding of biological neurons is that they communicate through pulses and employ the relative timing of the pulses to transmit information and perform computations. Spiking Neural Networks (SNNs) [41–43], known as the third generation of Artificial Neural Networks (ANNs), communicate by transmitting short transient spikes to other neurons, via weighted synaptic connections. SNNs differ from traditional neural network models in that they utilise both timing and magnitude dynamics for the processing of neural information. Maass [43] demonstrates mathematically that SNNs are computationally more powerful than traditional threshold-based neuron models. This result has consequently encouraged interest in

the area of SNNs, and their application to real-world classification problems [44].

### 3.2. Genetic Algorithms

A Genetic Algorithm (GA) [45] is a class of Evolutionary Algorithm, which incorporates the mechanisms of phylogenetic adaptation observed in nature. Guided by the "survival of the fittest" principle, GAs are global search algorithms that encode points in the solution space into a linear data string (genome). Apart from implementing the encoding mechanism and fitness function, GAs also have to perform the genetic operations. A GA includes three bio-inspired mechanisms to guide evolutionary search towards good solutions, namely:

- Survival of the fittest (selection)
- Recombination of parents' genes (crossover)
- Random variation (mutation)

Evolutionary techniques have been used to perform neural network topology design, synaptic weight training, weight initialization and learning rule/activation function selection [46]. SNN training using GAs has been successfully demonstrated by [47–49]. In this research, the evolution of SNN synaptic weights and neuron firing thresholds is investigated. The initial population of SNNs is randomly generated by the GA where the properties (synaptic input weights, neuron firing threshold) of each node are encoded in a data string or genome [50]. The resulting genome is used to configure and implement the corresponding SNN. Following fitness assessment and selection, the crossover operator recombines parts of each of the selected parent genomes to generate a new offspring individual. Random mutation of neural synaptic weights and neuron firing thresholds is then applied to introduce additional genetic diversity to the population. Elitism (preserving the best individual through each generation) is utilized by the GA. The GA parameters employed for this research are as detailed in [50].

## 4. EXPERIMENTAL SETUP

### 4.1. Principal Component Analysis

In order to extract the relevant features that will reflect the RTS of the tumours, it is important to use a feature extraction method such as the Principal Component Analysis (PCA). PCA reduces the dimensionality of multivariate data and reveals simplified structures that are often hidden in the original data set, while also disregarding

less relevant information such as noise or co-linearities in signals [51]. PCA allows for a new representation of the original data in which maximum variance is exposed, so that data may then be better discriminated. Mathematically, the basis that was used to record the original signals is changed, by means of a linear algebraic operation, into a new orthonormal basis that allows for the data to present maximal variance [51]. The resulting principal components are ordered by decreasing variance. It must be noted that PCA is non-parametric so only the data influences the PCA calculation disregarding any prior acquiring system or known labels.

### 4.2. Principal Component Preprocessing

SNNs map real world scalar data into spike train frequencies [52]. In this research, high PCA values are mapped to high spike frequencies while low PCA values are mapped to low frequencies. Since PCA values are scaled between $[-1, +1]$, it is necessary to decouple the positive and negative ranges of each PCA component (P(n)) into two spike generating inputs (P(n)+ and P(n)−). This decoupling ensures that a +1 PCA input generates the same number of spikes (and influence) on the SNN as a −1 PCA input, thus removing any bias from the encoding process.

### 4.3. SNN Breast Cancer Classifier System Architecture Application

Figure 3 illustrates the single-hidden-layer SNN architecture used to implement the SNN Breast Cancer Classifier. The SNN processes the first 12 PCA components (P1-P12). Twenty-four spike generators (SG1-SG24) are used to map real-valued PCA data into spike trains using a linear magnitude to (spike train) frequency conversion [52]. This PCA spike data is fed to the network's 24 hidden layer neurons (N1-N24). Two output layer spiking neurons (N25, N26) generate two spike trains, the outputs of which determine the system's classification. Two spike counters (SC1, SC2) are employed to count the number of output spikes (within a given update interval) [52]. Counter values C1 and C2 are used to determine classifier behavior. The counter with the largest spike count value designates the selected class. Each spiking neuron is fully forward connected to the next SNN layer. The neuron model chosen for these experiments is based on the leaky integrate and fire model [43]. Each SNN individual is composed of 26 genes, which correspond to the 26 evolvable spiking neurons (N1-N26). The spiking neuron parameters are configurable by the GA. Each gene contains 25 real-valued numbers: 24 input synaptic weights and 1 neuron

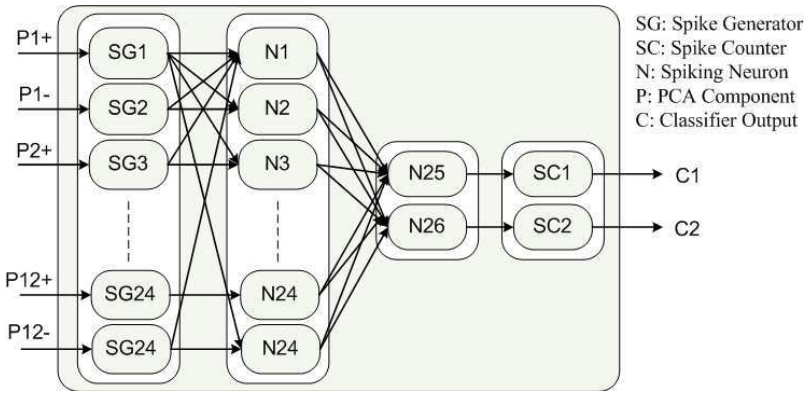


**Figure 3.** SNN architecture for SNN Breast Cancer Classifier System, illustrating PCA inputs (P1-P12), spike generators (SG1-SG24), spiking neurons (N1-N26), spike counters (SC1, SC2) and SNN classifier outputs (C1,C2).

firing threshold. Therefore, the genome consists of 650 real-valued entries. Synaptic weights range from $[-1.05, 1.05]$ while thresholds vary between $[0, 4.0]$ [50]. Fitness assessment of the SNN-based breast cancer classifier is achieved using a fitness function, which rewards individuals based on the number of correct classifications made. $C^m$ refers to the number of correct malignant classifications made by the SNN. $C^b$ refers to the number of correct benign classifications. $C_{\max}$ and $C_{\min}$ are defined in Equations (3) and (4).

$$C_{\max} = \max\left[C^m, C^b\right] \tag{3}$$

$$C_{\min} = \min\left[C^m, C^b\right] \tag{4}$$

The fitness, $f$, of the SNN is defined in Equation (5).

$$f = \left((C_{\min})^{\beta}\right) + C_{\max} \tag{5}$$

A $\beta$ value of 1.5 is employed in this research to reward the correct classification of both tumour classes. Without this fitness bias, fitness can be accumulated by classifying a single tumour class repeatedly. By including this bias, networks that select correctly from both classes are rewarded above networks that correctly select from just one class.

## 5. RESULTS AND CONCLUSIONS

A total of 368 tumour models were considered (184 of size 2.5 mm and 184 of size 7.5 mm). Within that group, there were 184 type 1 tumours (malignant), 92 type 2 tumours (macrolobulated benign) and 92 type 3 tumours (smooth benign). Two different classifier architectures are considered:

(i) A direct "type" classifier that simply classifies each tumour as either benign or malignant

(ii) A two-stage classifier that classifies each tumour as either small or large, before classifying the tumours as either benign or malignant.

These simple classifier architectures have been previously examined by both Davis and Conceição et al. [33–35, 53]. The tumour backscatter is classified using the SNN, but also using Linear Discriminant Analysis (LDA) [33]. The reason LDA is also used is that it provides a useful baseline when examining the performance and robustness of the SNN classifier. LDA has previously been examined by both Davis and Conceicao et al. and is based on the assumption that the groups being discriminated have multivariate normal distributions and have the same covariance matrix. With the LDA method, the pooled within-group covariance matrix is calculated and used to determine the discriminant function which will allow classification. In order to evaluate both classification methods, the entire data-set is randomly shuffled and divided into 75%–25% training and test groups respectively. This classification process is repeated 10 times and the average performance of each classifier is calculated. The results are presented in Table 1. For the direct classifier, the SNN outperformed the LDA classifier by approximately 12% (82.30% for LDA compared to 94% for the SNN). Examining the two stage Size-then-Type classifier, the SNN outperformed the LDA classifier in terms of both size and type classification. For size classification, the SNN had an accuracy of 99.5% compared to 91.2% for the LDA classifier. Furthermore, in terms of type, the SNN once again provided improved results, outperforming the LDA classifier by almost 8%. Overall, the best performing classifier

**Table 1.** Results of one and two stage classifier.

| Classifier | One-Stage Type (%) | Two-Stage Size (%) | Two-Stage Type (%) |
|---|---|---|---|
| LDA | 82.30 | 91.2 | 90.69 |
| SNN | 94 | 99.5 | 98.71 |

architecture was the two stage SNN classifier, with an overall type accuracy of almost 99%.

Linear classifiers such as LDA can only partition classes using a hyperplane [54]. This technique works well if the classes are linearly separable, however, real-world classification tasks are not always characterised by a linearly separable feature space. This linear inseparability is evident with the classic XOR function, where no hyperplane exists that partitions both classes correctly [54]. The demand for non-linear classification motivated the development of multi-layered perceptron (MLP) neural networks. MLPs can approximate any non-linear function and therefore can partition a feature space in a non-linear fashion [55]. With regard to spiking neurons, Maass demonstrated that multi-layer SNNs can also approximate any non-linear function and are computationally more powerful than traditional artificial neuron models [43]. An SNN's ability to partition classes that are not strictly linearly separable can explain their superior performance compared to LDA. In addition a GA's global search ability avoids the problem of being trapped at a local sub-optimal solution that local-search neural network training algorithms such as back-propagation may encounter.

Future work will examine the performance of the SNN classifier in a more dielectrically heterogeneous breast, where the tumour RTS could be masked due to clutter in the resultant UWB signals.

## ACKNOWLEDGMENT

This work is supported by Science Foundation Ireland (SFI) under grant numbers 07/RFP/ENEF420 and 07/SRC/I1169.

## REFERENCES

1. Dixon, M. J., *ABC of Breast Diseases*, Wiley-Blackwell, 2006.
2. Nass, S. L., I. C. Henderson, and J. C. Lashof, *Mammography and Beyond: Developing Technologies for the Early Detection of Breast Cancer*, National Academy Press, 2001.
3. Bird, R. E., T. W. Wallace, and B. C. Yankaskas, "Analysis of cancers missed at screening mammograph," *Radiology*, Vol. 184, 613–617, 1992.
4. Huynh, P. H., A. M. Jarolimek, and S. Daye, "The false-negative mammogram," *RadioGraphics*, Vol. 18, 1137–1154, 1998.
5. Elmore, J. G., M. B. Barton, V. M. Moceri, S. Polk, P. J. Arena, and S. W. Fletcher, "Ten-year risk of false positive screening

mammograms and clinical breast examinations," *New Eng. J. Med.*, Vol. 338, No. 16, 1089–1096, 1998.

6. Hall, F. M., J. M. Storella, D. Z. Silverstone, and G. Wyshak, "Non-palpaple breast-lesions, recommendations for biopsy based on suspicion of carcinoma at mammography," *Radiology*, Vol. 167, No. 2, 353–358, 1988.
7. Wang, L., X. Zhao, H. Sun, and G. Ku, "Microwave-induced acoustic imaging of biological tissues," *Rev. Sci. Instrum.*, Vol. 70, No. 9, 3744–3748, 1991.
8. Li, D., P. M. Meaney, T. Raynolds, S. A. Pendergrass, M. W. Fanning, and K. D. Paulsen, "Parallel-detection microwave spectroscopy system for breast cancer imaging," *Rev. Sci. Instrum.*, Vol. 75, No. 7, 2305–2313, 2004.
9. Kruger, R. A., K. D. Miller, H. E. Reynolds, W. L. Kiser, D. R. Reinecke, and G. A. Kruger, "Breast cancer in vivo: Contrast enhancement with thermoacoustic CT at 434 MHz — Feasibility study," *Radiology*, Vol. 216, No. 1, 279–283, 2000.
10. Bulyshev, A., S. Y. Semenov, A. E. Souvorov, R. H. Svenson, A. G. Nazorov, Y. E. Sizov, and G. P. Tatsis, "Computational modeling of three-dimensional microwave tomography of breast cancer," *IEEE Trans. Biomed. Eng.*, Vol. 48, No. 9, 1053–1056, Sep. 2001.
11. Meaney, P. M., M. W. Fanning, D. Li, S. P. Poplack, and K. D. Paulsen, "A clinical prototype for active microwave imaging of the breast," *IEEE Trans. Microwave Theory Tech.*, Vol. 48, No. 11, 1841–1853, Nov. 2000.
12. Meaney, P. M., K. D. Paulsen, J. T. Chang, M. W. Fanning, and A. Hartov, "Nonactive antenna compensation for fixed-array microwave imaging: Part II — Imaging results," *IEEE Trans. Med. Imag.*, Vol. 18, No. 6, 508–518, Jun. 1999.
13. Souvorov, A. E., A. E. Bulyshev, S. Y. Semenov, R. H. Svenson, and G. P. Tatis, "Two-dimensional analysis of a microwave flat antenna array for breast cancer tomography," *IEEE Trans. Microwave Theory Tech.*, Vol. 48, No. 8, 1413–1415, Aug. 2000.
14. Hagness, S. C., A. Taflove, and J. E. Bridges, "Two-dimensional FDTD analysis of a pulsed microwave confocal system for breast cancer detection: Fixed-focus and antenna-array sensors," *IEEE Trans. Biomed. Eng.*, Vol. 45, No. 12, 1470–1479, 1998.
15. Daniels, D. J., *Surface Penetrating Radar*, IEE Press, London, 1996.
16. Hagness, S. C., A. Taflove, and J. E. Bridges, "Three-dimensional

FDTD analysis of a pulsed microwave confocal system for breast cancer detection: Design of an antenna-array element," *IEEE Trans. Antennas and Propagat.*, Vol. 47, No. 5, 783–791, May 1999.

17. Fear, E. C., X. Li, S. C. Hagness, and M. A. Stuchly, "Confocal microwave imaging for breast cancer detection: Localization of tumors in three dimensions," *IEEE Trans. Biomed. Eng.*, Vol. 49, No. 8, 812–822, Aug. 2002.
18. Fear, E. C. and M. A. Stuchly, "Microwave system for breast tumor detection," *IEEE Microwave and Guided Wave Letters*, Vol. 9, No. 11, 470–472, Nov. 1999.
19. Fear, E. C., J. Sill, and M. A. Stuchly, "Experimental feasibility study of confocal microwave imaging for breast tumor detection," *IEEE Trans. Microwave Theory Tech.*, Vol. 51, No. 3, 887–892, Mar. 2003.
20. Fear, E., J. Sill, and M. Stuchly, "Microwave system for breast tumor detection: Experimental concept evaluation," *IEEE AP-S International Symposium and USNC/URSI Radio Science Meeting*, Vol. 1, 819–822, San Antonio, Texas, Jun. 2002.
21. Li, X. and S. C. Hagness, "A confocal microwave imaging algorithm for breast cancer detection," *IEEE Microwave and Wireless Components Letters*, Vol. 11, No. 3, 130–132, 2001.
22. Bond, E. J., X. Li, S. C. Hagness, and B. D. V. Veen, "Microwave imaging via space-time beamforming for early detection of breast cancer," *IEEE Trans. Antennas and Propagat.*, No. 8, 1690–1705, Aug. 2003.
23. Xie, Y., B. Guo, J. Li, and P. Stoica, "Novel multistatic adaptive microwave imaging methods for early breast cancer detection," *EURASIP J. Appl. Si. P.*, Vol. 2006, Article ID: 91961, 1–13, 2006.
24. Guo, B., Y. Wang, J. Li, P. Stoica, and R. Wu, "Microwave imaging via adaptive beamforming methods for breast cancer detection," *PIERS Online*, Vol. 1 No. 3, 350–353, Hangzhou, China, 2005.
25. Lazebnik, M., L. McCartney, D. Popovic, C. B. Watkins, M. J. Lindstrom, J. Harter, S. Sewall, A. Magliocco, J. H. Booske, M. Okoniewski, and S. C. Hagness, "A large-scale study of the ultrawideband microwave dielectric properties of normal breast tissue obtained from reduction surgeries," *Phys. Med. Biol.*, Vol. 52, 2637–2656, 2007.
26. Lazebnik, M., D. Popovic, L. McCartney, C. B. Watkins, M. J. Lindstrom, J. Harter, S. Sewall, T. Ogilvie, A. Magliocco,

T. M. Breslin, W. Temple, D. Mew, J. H. Booske, M. Okoniewski, and S. C. Hagness, "A large-scale study of the ultrawideband microwave dielectric properties of normal, benign and malignant breast tissues obtained from cancer surgeries," *Phys. Med. Biol.*, Vol. 52, 6093–6115, 2007.

27. O'Halloran, M., M. Glavin, and E. Jones, "Effects of fibroglandular tissue distribution on data-independent beamforming algorithms," *Progress In Electromagnetics Research*, Vol. 97, 141–158, 2009.
28. Chen, Y., E. Gunawan, K. S. Low, S. Wang, C. Soh, and J. Lavanya, "Effect of lesion morphology on microwave signature in ultra-wideband breast imaging: A preliminary two-dimensional investigation," *IEEE Antennas and Propagation Society International Symposium*, 2168–2171, 2007.
29. Chen, Y., I. Craddock, and P. Kosmas, "Feasibility study of lesion classification via contrast-agent-aided uwb breast imaging," *IEEE Transactions on Biomedical Engineering*, Vol. 57, No. 5, 1003–1007, 2010.
30. Chen, Y., I. Craddock, P. Kosmas, M. Ghavami, and P. Rapajic, "Application of the mimo radar technique for lesion classification in UWB breast cancer detection," *17th European Signal Processing Conference (EUSIPCO)*, 759–763, 2009.
31. Chen, Y., I. J. Craddock, P. Kosmas, M. Ghavami, and P. Rapajic, "Multiple-input multiple-output radar for lesion classification in ultrawideband breast imaging," *IEEE Journal of Selected Topics in Signal Processing*, Vol. 4, No. 1, 187–201, 2010.
32. Chen, Y., E. Gunawan, K. S. Low, S. C. Wang, C. Soh, and T. Choudary, "Effect of lesion morphology on microwave signature in 2-D ultra-wideband breast imaging," *IEEE Transactions on Biomedical Engineering*, Vol. 55, No. 8, 2011–2021, 2008.
33. Conceição, R. C., D. Byrne, M. O'Halloran, E. Jones, and M. Glavin, "Investigation of classifiers for early-stage breast cancer based on radar target signatures," *Progress In Electromagnetics Research*, Vol. 105, 295–311, 2010.
34. Conceição, R. C., M. O'Halloran, M. Glavin, and E. Jones, "Support vector machines for the classification of early-stage breast cancer based on radar target signatures," *Progress In Electromagnetics Research B*, Vol. 23, 311–327, 2010.
35. Davis, S. K., B. D. V. Veen, S. C. Hagness, and F. Kelcz, "Breast tumor characterization based on ultrawideband backscatter," *IEEE Trans. Biomed. Eng.*, Vol. 55, No. 1, 237–246, 2008.
36. Nguyen, M. and R. Rangayyan, "Shape analysis of breast masses

in mammograms via the fractial dimension," *IEEE Engineering in Medicine and Biology 27th Annual Conference*, 3210–3213, 2005.

37. Muinonen, K., "Introducing the gaussian shape hypothesis for asteroids and comets," *Astronomy and Astrophysics*, Vol. 332, 1087–1098, 1998.
38. Muinonen, K., *Light Scattering by Stochastically Shaped Particles*, Chapter 11, Academic Press, 2000.
39. Taflove, A. and S. C. Hagness, *Computational Electrodynamics: The Finite-difference Time-domain Method*, Artech House Publishers, Jun. 2005.
40. Koch, C. and G. Laurent, "Complexity and the nervous system," *Science*, Vol. 284, No. 5411, 96–98, Washington, DC, 1999.
41. Maass, W., "Computation with spiking neurons," *The Handbook of Brain Theory and Neural Networks*, 1080–1083, 2003.
42. Gerstner, W. and W. Kistler, *Spiking Neuron Models*, Cambridge University Press, New York, 2002.
43. Maass, W., "Networks of spiking neurons: The third generation of neural network models," *Neural Networks*, Vol. 10, No. 9, 1659–1671, 1997.
44. Bohte, S., J. Kok, and H. La Poutre, "Error-backpropagation in temporally encoded networks of spiking neurons," *Neurocomput Ing.*, Vol. 48, No. 1–4, 17–37, 2002.
45. Holland, J., *Adaptation in Natural and Artificial Systems*, MIT Press, Cambridge, MA, 1992.
46. Yao, X., "Evolving artificial neural networks," *Proceedings of the IEEE*, Vol. 87, No. 9, 1423–1447, 1999.
47. Hagras, H., A. Pounds-Cornish, M. Colley, V. Callaghan, and G. Clarke, "Evolving spiking neural network controllers for autonomous robots," *IEEE International Conference on Robotics and Automation*, Vol. 5, 4620–4626, 2004.
48. Floreano, D., N. Schoeni, G. Caprari, and J. Blynel, "Evolutionary bits 'n' spikes," *Proceedings of the Eighth International Conference on Artificial Life*, 335–344, 2003.
49. Belatreche, A., L. P. Maguire, M. McGinnity, and Q. X. Wu, "Evolutionary design of spiking neural networks," *New Mathematics and Natural Computation (NMNC)*, Vol. 2, No. 03, 237–253, 2006.
50. Rocke, P., B. McGinley, J. Maher, F. Morgan, and J. Harkin, "Investigating the suitability of FPAAs for evolved hardware spiking neural networks," *Proceedings of Evolvable Systems: From*

*Biology to Hardware*, 118–126, 2008.

51. Wold, H., "Estimation of principal components and related models by iterative least squares," *Multivariate Analysis*, K. Krishnaiah, Ed., Academic Press, New York, 1996.
52. Pande, S., F. Morgan, C. S., B. McGinley, S. Carrillo, L. McDaid, and J. Harkin, "Embrace-sysc for analysis of noc-based spiking neural network architecture," *IEEE System on a Chip Symposium (SOC)*, 2010.
53. Davis, S. K., S. C. Hagness, and B. D. V. Veen, "Microwave-based detection of breast cancer using the generalized likelihood ratio test," *IEEE Workshop on Statistical Processing*, 617–620, 2003.
54. Theodoridis, S. and K. Koutroumbas, *Pattern Recognition*, Academic Press, 2006.
55. Hornik, K., M. Stinchcombe, and H. White, "Multilayer feedforward networks are universal approximators," *Neural Networks*, Vol. 2, No. 5, 359–366, 1989.